Available online at www.sciencedirect.com
SCIENCE DIRECT®
ELSEVIER
Earth and Planetary Science Letters 220 (2004) 391–408
EPSL
www.elsevier.com/locate/epsl

Sub-ice geology inland of the Transantarctic Mountains in light of new aerogeophysical data

Michael Studinger [a,*], Robin E. Bell [a], W. Roger Buck [a], Garry D. Karner [a], Donald D. Blankenship [b]

[a] *Lamont–Doherty Earth Observatory of Columbia University, Palisades, NY 10964, USA*
[b] *Institute for Geophysics, John A. and Katherine G. Jackson School of Geosciences, University of Texas at Austin, Austin, TX, USA*

Received 5 May 2003; received in revised form 8 January 2004; accepted 15 January 2004

Abstract

The Transantarctic Mountains are a major geologic boundary that bisects the Antarctic continent, separating the low-lying, tectonically active terrains of West Antarctica from the East Antarctic craton. A new comprehensive aerogeophysical data set, extending 1150 km from the Ross Sea into the interior of East Antarctica provides insights into the complex structure inland of the Transantarctic Mountains. Geophysical maps, compiled from 21 000 km of gravity, magnetic and subglacial topography data, outline the boundaries of several geologic and tectonic segments within the survey area. The coherent pattern in magnetic data and mesa topography suggests a subglacial extent of the Transantarctic Mountains 400–500 km inland the last exposed rock outcrops. We estimate the maximum thickness of a potential sediment infill in the Wilkes Subglacial Basin to be less than 1 km, based on gravity modeling and source depth estimates from magnetic data. The coherent nature of the potential field and topography data, together with the northwest–southeast trends, define the Adventure Subglacial Trench and the Resolution Subglacial Highlands as a tectonic unit. The crustal structure and the strong similarity of the observed gravity with fold-and-thrust belts suggest a compressional scenario for the origin of the Adventure Subglacial Trench and the Resolution Subglacial Highlands. The complexity and apparent structural control of the Wilkes Subglacial Basin raise the issue of what influence pre-existing structures may have played in the formation of the Transantarctic Mountains system. The previous hypothesis of a thermal boundary beneath the mountains is difficult to reconcile with our new gravity data. The apparent difficulties to match our new data with certain key aspects of previous models suggests that a reassessment of the existing uplift models is necessary. We have modeled the prominent gravity anomaly over the Transantarctic Mountains with thicker crust.

Keywords: Antarctica; Transantarctic Mountains; Wilkes Subglacial Basin; aerogeophysics; gravity; magnetics; radar echo sounding

1. Introduction

The Transantarctic Mountains, a more than 3500-km-long and 4500-m-high mountain range, mark the lithospheric and morphologic boundary

* Corresponding author. Tel.: +1-845-365-8598; Fax: +1-845-365-8179.
E-mail address: mstuding@ldeo.columbia.edu (M. Studinger).

0012-821X/04/$ – see front matter © 2004 Elsevier B.V. All rights reserved.
doi:10.1016/S0012-821X(04)00066-4

between the East Antarctic craton and an assemblage of allochthonous crustal blocks forming West Antarctica (Fig. 1) (e.g. [1,2]). The high relief of the Transantarctic Mountains flanks the low-lying Ross Embayment consisting of the Ross Sea, the Ross Ice Shelf, and the interior Ross Embayment. The Ross Embayment is comprised of several sedimentary basins of the West Antarctic rift system [3–5]. The extreme relief of the Transantarctic Mountains and the simplicity of their gently tilted structure has prompted a variety of models as to their origin. These models include a tilted block forming the uplifted hanging wall above a low-angle detachment fault [6], and a flexurally uplifted footwall of an unloaded plate edge bounded by a high-angle normal fault [7]. The cause for the uplift of the Transantarctic Mountains remains poorly understood.

On the backside of the Transantarctic Mountains a long-wavelength downwarp in subglacial topography has been interpreted as the Wilkes Subglacial Basin. This basin parallels the mountain range on the inland side and is thought to contain several kilometers of sediment infill [8]. Contrasting models for the origin of the Wilkes Subglacial Basin range from rifted crust [8–10] to a flexural origin [7,11]. The flexural models link the formation of the Wilkes Subglacial Basin to the Cenozoic uplift of the Transantarctic Mountains, while the rift model proposes a more recent origin of the Wilkes Subglacial Basin. Between the Wilkes Subglacial Basin and Dome C lies a 1500-m-deep and 50-km-wide trench, the Adventure

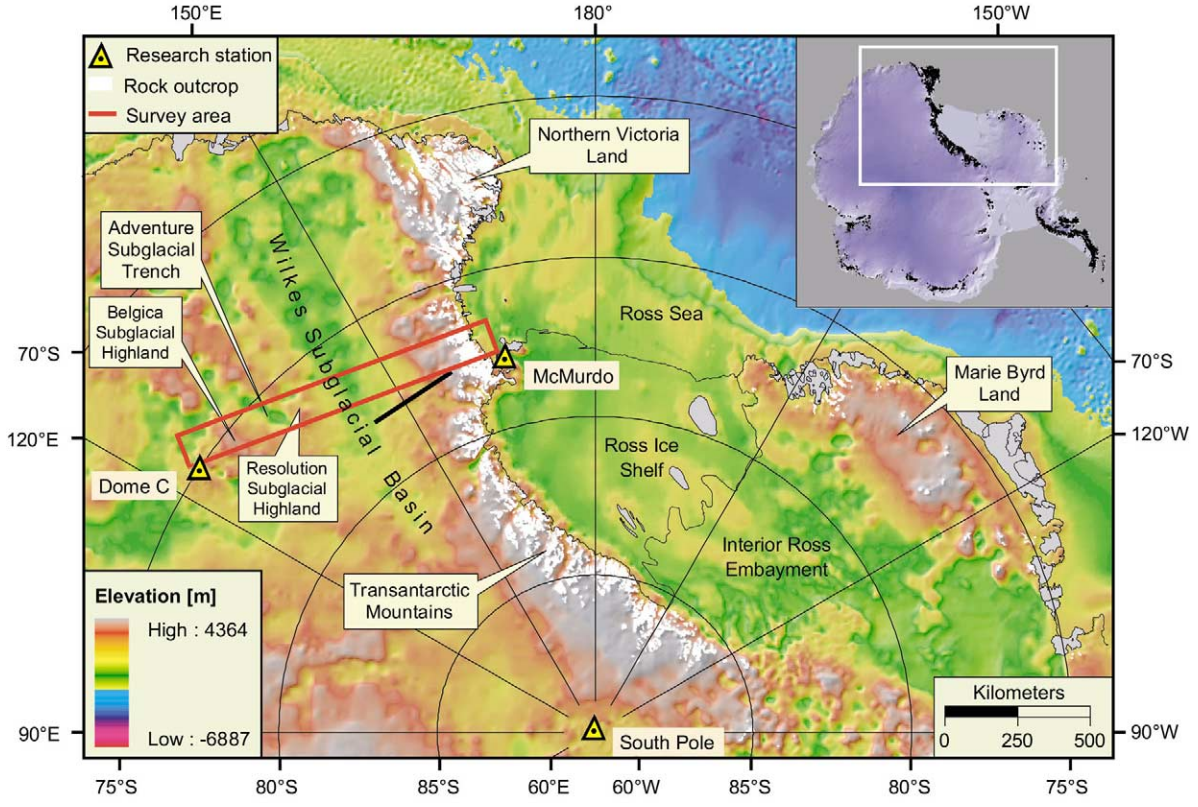

Fig. 1. Subglacial topography and bathymetry map of Antarctica [42]. The Ross Embayment comprises the Ross Sea, the Ross Ice Shelf and the Interior Ross Embayment. Black line marks location of EAST 93 traverse adjacent to the aerogeophysical survey area (red box) [11].

Subglacial Trench (Fig. 1). Drewry et al. [8], Steed and Drewry [9] and Ferraccioli et al. [10] proposed rifted crust beneath the trench and between 3 and 10 km of sediment infill. Data coverage over this structure is sparse and its origin remains unconstrained.

In order to understand the uplift of the Transantarctic Mountains, both the Ross Sea and the hinterland need to be included in the analysis. Over the past decades, the Ross Sea has been studied extensively, however, evidence is emerging that the existing geophysical models of the formation of the Ross Sea basins and their relationship to the Transantarctic Mountains need to be reassessed [12]. The sparse data coverage on the backside of the Transantarctic Mountains has precluded any comprehensive analysis of the geologic and tectonic structure of this region to date. The aim of this paper is to reassess the structure of the backside of the Transantarctic Mountains in light of new aerogeophysical data.

2. Aerogeophysical data

2.1. Survey design

We use a set of integrated airborne geophysical data collected onboard a ski-equipped DeHavilland Twin Otter aircraft operated by the US National Science Foundation's Support Office for Aerogeophysical Research (SOAR). The survey area covers 1150 by 116 km, ranging from McMurdo Sound towards Dome C (Fig. 1). In total, more than 21 000 line-km of gravity, magnetic and ice-penetrating radar data were acquired during the austral summer 1999/2000. The survey was flown on a grid with flight lines spaced 10.6 km apart and tie lines every 31.8 km. Additional profiles have been acquired for the southern half of the Dome C block resulting in a 5.3-km line spacing. The survey was flown at constant barometric altitudes. Flying heights were 3720 m for the Dome C block (western half of the survey grid) and 3050 m for the Transantarctic Mountains block (eastern half of the survey grid). Departures from these flying heights were occasionally necessary to avoid icing conditions or elevated terrain.

2.2. Positioning

The correction of large vertical accelerations for the gravity measurements demands high-precision positioning of the aircraft. Dual-frequency carrier phases of the Global Positioning System (GPS) were collected simultaneously at a 1-Hz rate by three receivers on the aircraft and three receivers at the base station. A differential carrier phase solution has been calculated for each flight using the Kinematic and Rapid Static (KARS) GPS package [13]. The root mean squared error estimate of all GPS solutions is below 0.04 m.

2.3. Magnetics

The total intensity of the Earth's magnetic field was recorded by a towed Cesium vapor magnetometer (a Geometrix 823A) at 10 Hz with an estimated precision of 0.001 nT. The 10-Hz data were down sampled to 1 Hz for data reduction which corresponds to an average spatial sampling distance of 70 m at an average ground speed of 70 m/s of the survey aircraft. The raw magnetic data have been corrected for diurnal variations recorded at magnetic base stations within the survey area. The International Geomagnetic Reference Field (IGRF) has been removed to obtain the total field anomaly. In order to improve the internal consistency of the magnetic data, we removed a trend of order two from the profile data. The standard deviation of the network adjusted crossover error is 18 nT. Differences in flight elevations have been compensated for by respective 2-D upward or downward continuation of the profiles to 3720 m for the Dome C block and 3050 m for the Transantarctic Mountains block. The composite grid was continued to a draped surface 3600 m above the subglacial topography using Cordell et al.'s method [14].

2.4. Gravity

A Bell Aerospace BGM-3 gravimeter, mounted on a gyro-stabilized platform, has been used for measuring relative changes in the Earth's gravity field. High-amplitude noise in the raw gravity data has been removed by low-pass filtering in

the frequency domain. The filter is a cosine taper that begins its roll-off at 0 Hz and reaches infinite attenuation at 0.006 Hz [15,16]. Vertical accelerations of the aircraft dominate the filtered raw gravity signal. The gravity signal of the vertical accelerations and the gravity effect of a moving platform on a rotating Earth are removed by applying an Eötvös correction for airborne measurements [17]. The resultant data are corrected with the latitude correction for the GRS-80 ellipsoid and the free-air correction to yield the free-air anomaly at the flight elevation. Crossover errors at intersections between flight lines and tie lines have been minimized by linear trend removal. The standard deviation of the network adjusted crossover error is 2.6 mGal. The free-air gravity measurements have been tied to the International Gravity Standardization Network (IGSN71) at McMurdo. The Transantarctic Mountains block free-air gravity grid was upward continued to 3720 m in the frequency domain in order to have a common flight elevation for the composite free-air gravity grid. The gridded free-air gravity and ice surface and subglacial topography data have been used to compile a Bouguer anomaly. We calculated the 3-D gravitational effect of the density contrast between the ice surface and air and between the bedrock and the ice sheet using Parker's frequency domain approach [18]. The series of Fourier transformations has been truncated after $N=7$ terms. Bulk densities of 900 kg m^{-3} and 2670 kg m^{-3} have been assumed for ice and bedrock respectively.

3. Topography, gravity and magnetic anomalies

3.1. Subglacial topography

The subglacial topography map has been compiled from ice surface elevation and ice thickness estimates derived from ice-penetrating radar data along profiles. The standard deviation of the crossover errors at intersections is 2.7 m for the ice surface elevation estimates and 81 m for the ice thickness estimates. Elevations are referenced to the WGS-84 ellipsoid. The subglacial topography shows several characteristic terrains. A step in topography from sea level to more than 2500 m around 163°E (km 1100 in Fig. 2a) marks the transition from the low-lying Ross Embayment to the Transantarctic Mountains front (Fig. 3b). A 400-km-long downwarp of the topography from the highest elevations (2000 m) to around −1000 m at 145°E (km 630 in Fig. 2a) defines the subglacial extent of the Transantarctic Mountains. The topographic low centered at 630 km is the axis of the Wilkes Subglacial Basin (WSB)

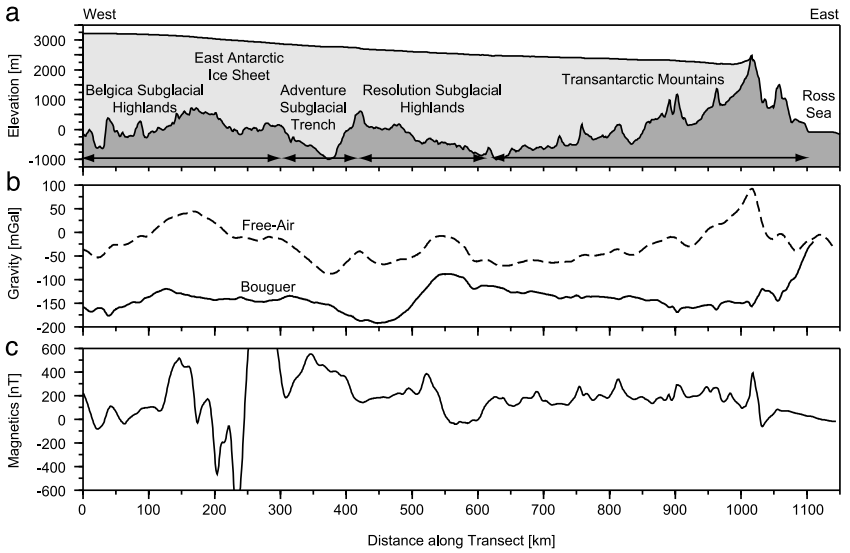

Fig. 2. Transect along the survey area. The profile is located in the center of the survey area of Fig. 1.

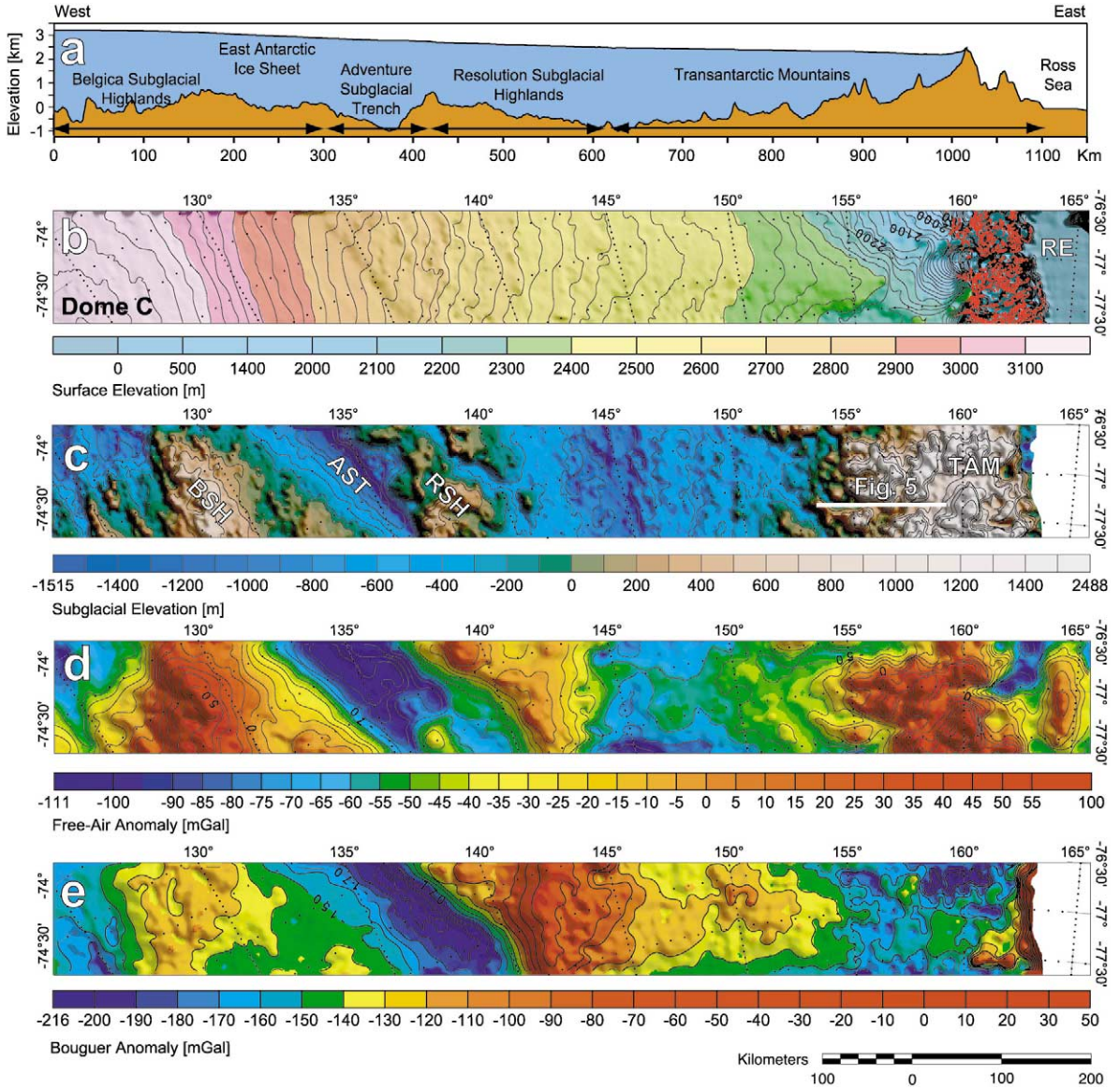

Fig. 3. (a) Transect across the survey area and distance scale for orientation. (b) Ice surface elevation in meters above sea level from ice-penetrating radar data. Red areas mark rock outcrops in the Transantarctic Mountains. Contour-line interval is 25 m above 2000 m. RE is Ross Embayment. (c) Subglacial topography in meters above sea level from ice-penetrating radar. Contour interval is 200 m. White line marks location of radar profile in Fig. 5. AST, Adventure Subglacial Trench; BSH, Belgica Subglacial Highlands; RSH, Resolution Subglacial Highlands; TAM, Transantarctic Mountains. (d) Free-air gravity anomaly in mGal. Contour-line interval is 10 mGal. (e) Bouguer anomaly in mGal.

[8,11,19]. To the west of this topographic low the topography increases to 500 m near 135°E (km 630–425 in Fig. 2a) forming the Resolution Subglacial Highlands (RSH). Near 135°E, the topography drops from 500 m down to −1000 m (km 425 in Fig. 2a). This steep, 60–80-km-wide trench is known as the Adventure Subglacial Trench (AST). Throughout the survey area, the eastern slope of this trench is consistently steeper than its western slope. West of the Adventure Subgla-

cial Trench, the subglacial topography varies between −500 and 1000 m and is part of the Belgica Subglacial Highlands (BSH).

3.2. Free-air and Bouguer gravity

A distinct change in Bouguer gravity (Fig. 3e) from around 0 to −125 mGal near 163°E marks the transition from the Ross Embayment to the Transantarctic Mountains (km 1100–1000 in Fig. 2b). West of the Transantarctic Mountains, the Bouguer gravity increases in a smooth slope from −150 to −75 mGal (km 900–550 in Fig. 2b). Earlier studies observed distinct Bouguer and free-air gravity anomalies over the Wilkes Subglacial Basin to the north [8]. No Bouguer or free-air anomaly is observed in this crossing of the Wilkes Subglacial Basin. The Bouguer gravity shows a pronounced up to −200 mGal low 100 km east of the Adventure Subglacial Trench. West of the Adventure Subglacial Trench, the Bouguer gravity shows a plateau with a slight increase towards −125 mGal over the Belgica Subglacial Highlands. West of the Belgica Subglacial Highlands, the Bouguer gravity decreases to −175 mGal.

3.3. Magnetics

The magnetic anomaly map shows a wide variety of characteristic wavelengths and amplitudes indicating changes in subglacial geology (Fig. 4). Beginning in the east over McMurdo Sound (162–166°E), the magnetic field is very smooth with amplitudes around zero (km 1150–1050 in Fig. 2c). Over the Transantarctic Mountains, the anomaly field is dominated by circular short-wavelength (5–20 km) high-amplitude (up to 500 nT) anomalies (around 160°E). Some of these anomalies are aligned north–south while others are isolated peaks. These short-wavelength anomalies are probably caused by doleritic dykes and sills in the Transantarctic Mountains. Previous workers noted that the Transantarctic Mountains do not have a corresponding magnetic anomaly in contrast to other orogenic mountain belts [20,21].

A distinct change in magnetic character, running from 157°E in the north to 160°E in the south, marks the boundary between the smooth field over the Transantarctic Mountains–McMurdo Sound area and the high amplitude magnetic field over the back side of the Transantarctic Mountains from 143°E to 157°E. The magnetic field over the backside is a composite of short- and long-wavelength anomalies with almost entirely positive amplitudes. The long-wavelength anomalies are of the order of 100 km and up to 250 nT and represent most likely sources between 10 km and the Curie Point isotherm. This long-wavelength structure is modulated by short-wavelength (5–10 km) low-amplitude (±50 nT) anomalies indicating shallow sources (Fig. 3). West of 143°E, the texture of the magnetic anomalies changes to a smooth long-wavelength pattern. This pattern is only disrupted by a high-amplitude negative–positive couple between 128°E and 136°E. The peak-to-through amplitudes on the profile data are as high as 3600 nT. Given the average distance between the source rocks and the sensor is around 3.5 km in this area, the peak-to-through amplitude of these anomalies is extraordinary. The observed high-amplitude structure is at the edge of the survey area and only a small part of the structure is mapped. The large distance to rock outcrops and other known tectonic features makes a reliable interpretation with respect to the geologic nature difficult.

3.4. Enhancement of magnetic data

In order to aid geologic interpretation potential field data are often analytically transformed to enhance certain characteristics which are diagnostic of the structural and geologic setting within the survey area.

The magnitude of the horizontal gradient of the total field anomaly enhances the structural trends in the magnetic data. The horizontal gradient acts as a high-pass filter which enhances shallow source lineaments in the magnetic data. The trend of the maxima and minima and lineaments follow the edges of source bodies with different magnetization. Thus, the lineaments in the horizontal gradient map reflect the structural trends of the shallow subglacial lithology.

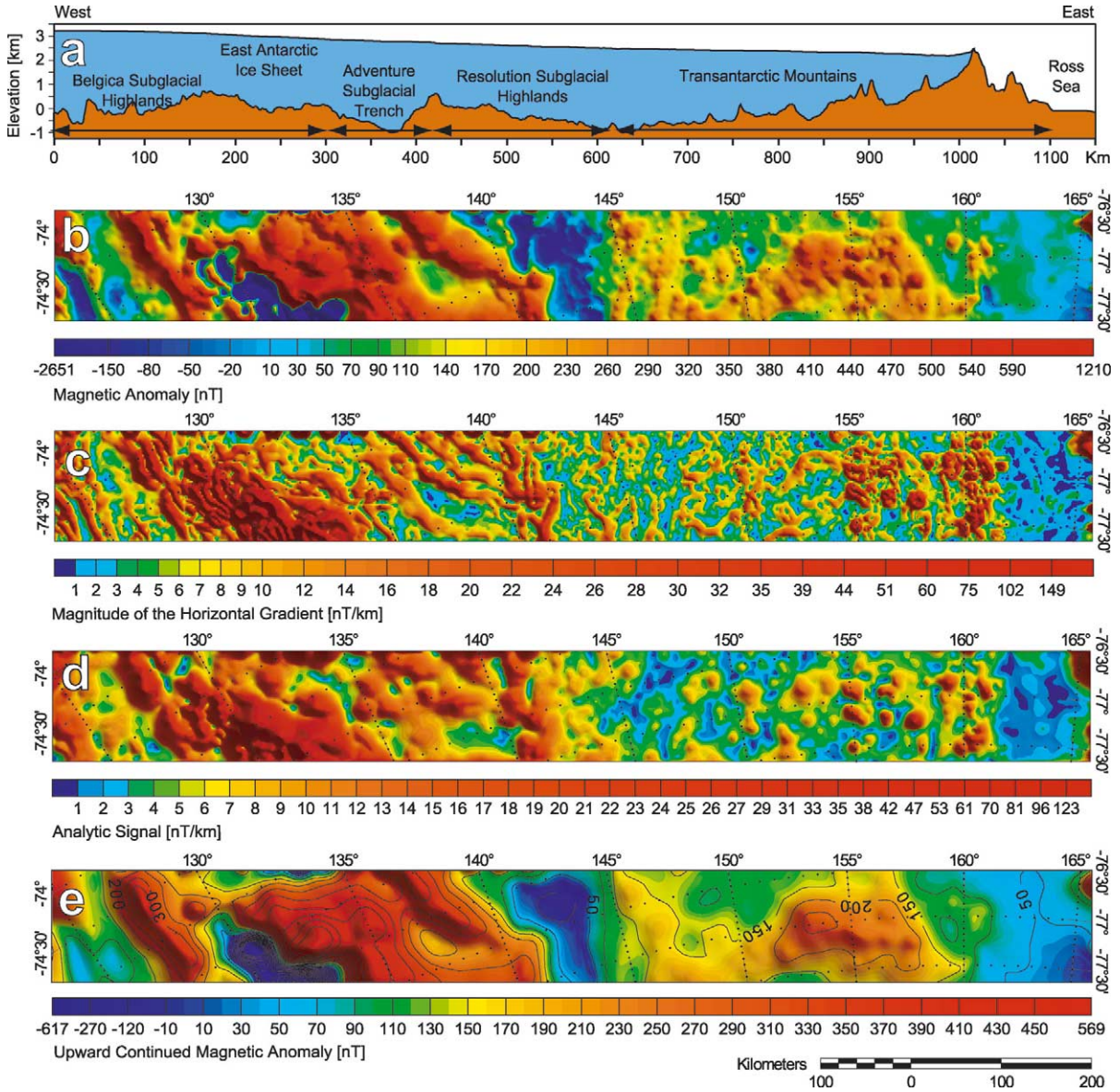

Fig. 4. (a) Transect across the survey area and distance scale for orientation. (b) Total field magnetic anomaly in nT, draped 3600 m onto the subglacial topography. (c) Amplitude of the horizontal gradient of the total field anomaly. (d) Analytic signal of magnetic anomaly. (e) 10 km upward continued magnetic anomaly in nT.

The absolute value of the 3-D analytic signal is defined as the square root of the squared sum of the vertical and the two horizontal derivatives of the magnetic field [22]. The shape and absolute value of the amplitude of the analytic signal are independent of the direction of magnetization and of the Earth's magnetic field. The absolute value of the 3-D analytic signal has maxima over magnetic contacts. In addition to being an interpretational aid, the analytic signal can also be used to estimate the depth to the source. The half width of the bell-shaped analytic signal roughly equals the depth to the magnetic source [22,23].

Upward continuation of the total magnetic field

accentuates anomalies caused by deep sources and attenuates anomalies caused by shallow sources. In particular, this technique can be utilized to remove the magnetic signal from the Jurassic doleritic sills and dykes of the Ferrar Group over the Transantarctic Mountains and their hinterland. The result is a magnetic map which reflects deeper sources. Long-wavelength magnetic anomalies most likely reflect the pattern of crustal magnetization (induced and remanent) down to the level of the Curie isotherm at 30–60 km in continental regions. However, long-wavelength magnetic anomalies can be caused by sources at any level in the crust (e.g. [24]).

3.5. Synoptic view

The horizontal gradient, the analytic signal, and the upward continued magnetic field all show similar structures which coincide with patterns in the subglacial topography and Bouguer gravity maps (Figs. 3 and 4). In order to remove the effect of the distance between source and receiver we use the magnetic field draped 3600 m above the subglacial topography as input. The illuminated surface of the horizontal gradient enhances the structural trend and the short-wavelength structure of the magnetic data. Between the eastern boundary of the survey grid and 162°E, the horizontal gradient shows a very smooth, featureless area, probably caused by the sediment cover of the Ross Embayment. Between 162°E and 142°E the horizontal gradient forms a short-wavelength, high frequency pattern. This pattern continues over the previously proposed location of the Wilkes Subglacial Basin (near 145°E) and does not show the typical smooth and quiet pattern observed over sedimentary basins for example east of the mountain front over the Ross Embayment. Further to the west, between 142°E and the western boundary of the survey grid the horizontal gradient develops a structural texture which aligns NS to NW–SE. The structure is formed by elongated ridges and troughs which have much longer wavelengths than the pattern observed over the Transantarctic Mountains. The orientation of these lineaments coincides with the main trends observed in the subglacial topography and Bouguer gravity (Fig. 3). Within this region, two smooth areas can be observed: the first one is located between 135°E and 140°E. This smooth area coincides with a distinct low in Bouguer anomaly (Fig. 3e) and could be an indication for sediment infill. The second smooth area is located between 125°E and 127°E. This structure is along the transition from a high to a low in the Bouguer gravity.

The analytic signal outlines a similar structural pattern as the horizontal gradient (Fig. 4). The area east of 162°E shows very smooth, low amplitude structure. Between 162°E and 142°E the analytic signal is comprised of circular, short wavelength anomalies of intermediate amplitude. The half width of the circular anomalies reflects source depths close to the ice–bedrock transition and slightly deeper. West of 162°E the half width of the analytic signal increases significantly, indicating deeper sources. The features in the analytic signal are oriented NS to NW–SE. The amplitudes are larger than over the Transantarctic Mountains and the Ross Sea.

The long-wavelength magnetic anomalies visible in the upward continued magnetic field support the concept that the boundaries identified in the magnetics, the horizontal gradient and the analytic signal outline major coherent crustal units within the survey area (Fig. 4). The same boundaries can be observed in the long-wavelength anomalies. However, the locations of these boundaries are less well defined due to the lower frequency content of the upward continued field. Over the Ross Embayment (east of 162°E) the upward continued magnetic field shows very small amplitudes (around 50 nT). The Transantarctic Mountains block (between 162°E and 142°E) shows amplitudes around 150 nT. The highest amplitudes in the long-wavelength field are observed west of 142°E.

4. Tectonic and geologic segments

On the basis of textural differences in subglacial topography, gravity and magnetic anomalies, the survey area can be divided into several segments, each representing a tectonic/geologic unit.

4.1. Transantarctic Mountains

Previous workers used the subglacial mesa topography observed on ice-penetrating radar profiles to estimate the subglacial extent of the Transantarctic Mountains [25]. The terraced morphology is thought to be caused by Ferrar dolerite sills overlying the sedimentary strata of the Beacon Supergroup [25]. Within our survey area we can also identify this topographic pattern diagnostic for the Transantarctic Mountains on several radar profiles (Fig. 5). Both, the coherent pattern in magnetic anomalies and the topographic signature from 160°E to 145°E support the idea that this unit represents the subglacial extent of the Transantarctic Mountains. The topographic signature and the magnetic anomalies may be caused by rocks of the Beacon Supergroup and the Ferrar sills. We modeled the magnetic effect of a thin layer of sill on top of the mesa topography (Fig. 5). The shape of the observed magnetic anomaly over two of the mesa structures (between km 70 and 85 and between 90 and 100) suggests a close correlation with the subglacial topography. Magnetic susceptibilities for the Ferrar Dolerites vary more than one order of magnitude [26]. We used susceptibilities which are close to the average value for the present-day magnetic field. Our apparent susceptibilities include remanent magnetization which according to Bull et al. [27] is polarized in the same direction as the present-day magnetic field. Higher or lower apparent susceptibilities would only result in a thinner or thicker layer of the causative model

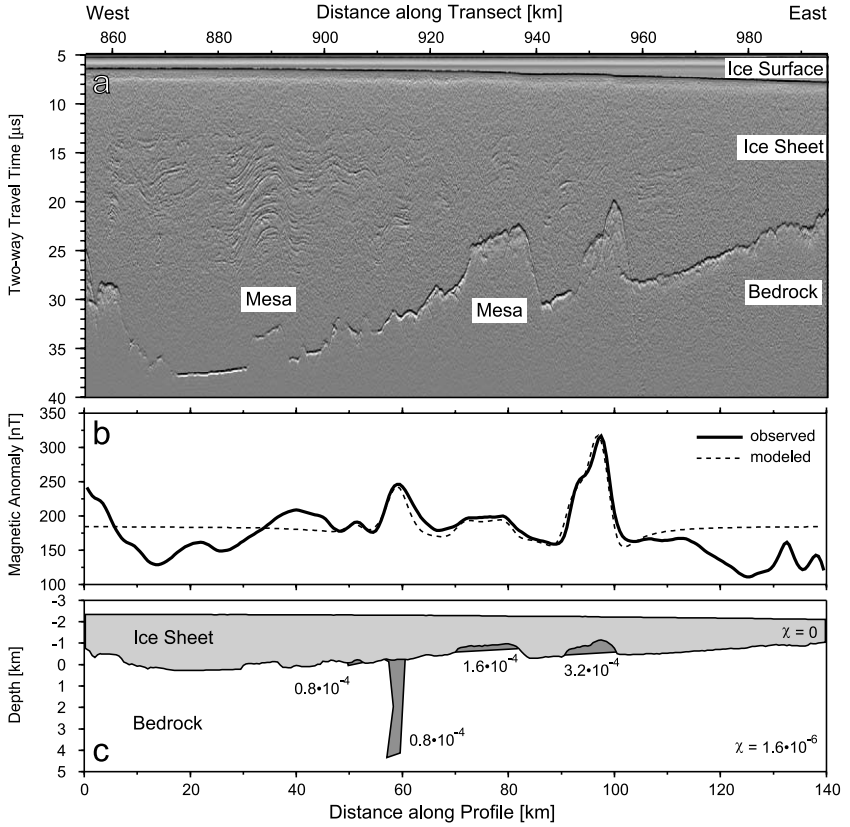

Fig. 5. (a) Ice-penetrating radar profile showing the mesa structure of the subglacial topography inland of the region with exposed rock outcrops. A scale using the distance along the transect has been added to aid comparison with all other figures. For location of profile see Fig. 3b. (b) Observed and modeled magnetic anomaly. (c) Magnetic model used to calculate the effect of Ferrar dolerites. Apparent susceptibilities χ are in SI units.

bodies. The surrounding rocks have been assigned the average weak susceptibility $\chi = 1.6\ 10^{-6}$ (SI units) of the Beacon group [26] and $\chi = 0$ for the ice sheet, respectively. We intended to keep the magnetic model as simple as possible and focus only on the origin of the short-wavelength anomalies. We are not concerned about the magnetic anomalies observed at the beginning of the profile (km 0–40 in Fig. 5) and at the eastern end (km 110–140). The observed magnetic anomaly over the mesa structure can be modeled by a thin layer of Ferrar dolerite sills. Near km 60, a dyke source explains the observed magnetics. The magnetic model confirms the interpretation of Steed [25] that the mesa structure is probably created by Ferrar dolerites on top of Beacon Group sediments. However, we also observed mesa topography not associated with magnetic anomalies (km 30–35 in Fig. 5). The magnetic model supports our interpretation that the short-wavelength anomalies are most likely caused by the subglacial extent of the Ferrar dolerites. Based on the coherent pattern in magnetic data and mesa topography the Transantarctic Mountains continue beneath the ice for at least 400–500 km from the last rock outcrops near 160–145°E (Fig. 3).

4.1.1. Endmember models for the response to loads

Modeling of the free-air gravity anomaly across the Transantarctic Mountains can offer insight into the mechanisms responsible for their formation and the density structure beneath the mountains. We have investigated the gravity effect of both, the long-wavelength gravity variations predominantly caused by the topography of the crust–mantle boundary, and by lateral changes in the deeper density structure. First, we calculate the gravity effect of two mechanical endmember scenarios for the response of the lithosphere to applied geological loads: Airy isostasy, a local isostatic scheme, that supports topography via crustal thickening, and second, a model that calculates the flexural response to loads near the mountain front.

A flexurally weak lithosphere (Airy model) supports a topographic load by local compensation at the crust–mantle boundary. The ice cover behind the Transantarctic Mountains plays a significant role in loading the lithosphere and we assume that the ice sheet has been in place long enough for the system to achieve isostatic equilibrium. For local compensation, the crustal thickness change in response to the load can be calculated:

$$\Delta z_{moho} = -(h_{ice}\rho_{ice} + z_{bedrock}\rho_{crust})/(\rho_{mantle} - \rho_{crust}) \quad (1)$$

where h_{ice} is the ice thickness, $z_{bedrock}$ is the elevation of the bedrock topography, ρ_{ice} is the average bulk density of the ice sheet, and ρ_{crust} and ρ_{mantle} are the densities of crust and mantle. Densities for the ice sheet, crust, and mantle are 900 kg/m^3, 2800 kg/m^3, and 3400 kg/m^3, respectively. The absolute depth of the crust–mantle boundary was tied to known crustal thickness estimates from teleseismic receiver functions (e.g. [28], around 35–40 km). Our gravity modeling, however, is generally insensitive to the absolute depth of the Moho.

The Moho topography of the second endmember model, the flexural unloading of an semi-infinite elastic plate, is fundamentally different from the Airy model. If the Transantarctic Mountains represent a flexural rift flank engendered by Ross Embayment extension, the Moho topography should generally parallel the topography of the uplifted rift shoulder [11]. The vertical deflection $W(x)$ of a lithospheric plate under a load P per unit area can be described with the following differential equation (thin plate approximation) (e.g. [29]):

$$D \cdot \nabla^4 W(x) + \Delta\rho \cdot g \cdot W(x) = P \quad (2)$$

where D is the flexural rigidity, $\Delta\rho$ is the density contrast, and g is the gravitational acceleration. The flexural rigidity D is related to the effective elastic thickness T_e by:

$$D = \frac{ET_e^3}{12 \cdot (1-\nu^2)} \quad (3)$$

where E is Young's modulus and ν is Poisson's ratio. Ten Brink et al. [11] assumed a broken or semi-infinite plate with the East Antarctic lithosphere having a free edge at the Transantarctic Mountains front. Using the boundary conditions

for a broken plate, Eq. 2 can be solved with a finite difference method allowing for lateral variations in flexural rigidity and load distribution. In our calculations we use the same load distribution as ten Brink et al. [11]: a load resulting from thermal buoyancy, an erosional load, the load of the ice sheet, and an isostatic end load ([11], fig. 7 herein). The only exception is that our ice load has been calculated using the observed ice thickness from radar data rather than the simplified geometry of ten Brink et al. [11]. The difference in the calculated flexural response between the two loads, however, is very small. Following ten Brink et al. [11], T_e increases linearly from $T_e = 5$ km at the coast to $T_e = 85$ km 130 km inland from the coast.

Fig. 6 shows the computed gravity assuming Airy and flexural unloading schemes for the Moho topography across the study area. The Airy model fits the gravity for the Transantarctic Mountains much better than the flexural unloading scheme. The gravity for the flexural unloading model differs significantly from the observed free-air gravity across the Transantarctic Mountains.

Fig. 6 illustrates the need for low density material beneath the Transantarctic Mountains in order to match the observed and modeled gravity. Ten Brink et al. [11] hypothesize that the long-wavelength gravity effect that results from the juxtaposition of two different crustal and lithospheric regions is the source of the lower gravity anomalies observed over the Transantarctic Mountains. The density change $\Delta\rho$ between the Ross Embayment and East Antarctica, related to the temperature change ΔT is:

$$\Delta\rho = \rho_0(1-\alpha\Delta T) \quad (4)$$

where ρ_0 is the East Antarctic mantle density (3350 kg/m^3), $\alpha = 3.4\cdot10^{-5}$ K^{-1} is the coefficient of thermal expansion, and ΔT is the temperature change in the mantle (285°K) [11]. This temperature induced density change proposed by ten Brink et al. ([11], fig. 9 herein) is difficult to reconcile with our observed gravity anomaly (Fig. 7).

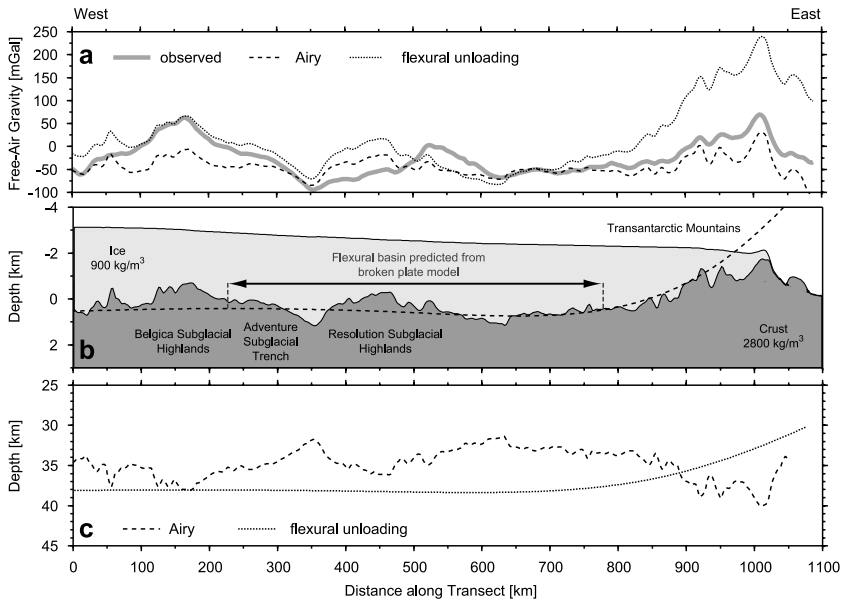

Fig. 6. 2-D free-air gravity models along the profile. (a) Observed and modeled free-air gravity. (b) View of the upper crust and ice sheet. Superimposed onto the observed topography is the modeled flexural response of the broken plate under load (dashed line). The flexural basin predicted from modeling is between km 220 and 790. (c) Moho topography used to model gravity. The absolute depth of the crust–mantle boundary was tied to known crustal thickness estimates from teleseismic receiver functions (e.g. [28], around 35–40 km) near km 900. The predicted gravity has been tied to the observed gravity at km 630.

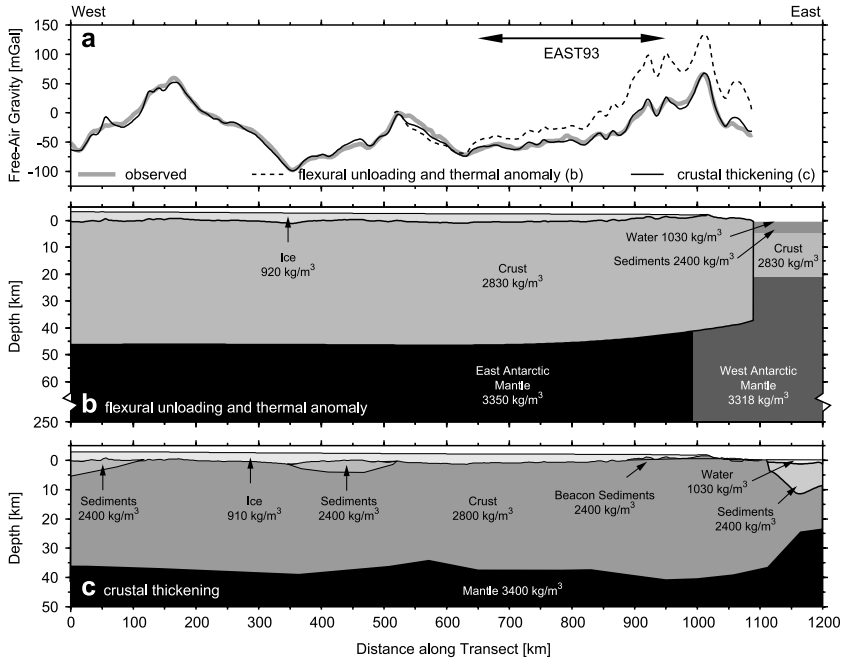

Fig. 7. 2-D free-air gravity models. (a) Observed and modeled free-air gravity. The approximate location of the EAST93 traverse [11] has been projected onto the profile. For exact location see Fig. 1. (b) Density distribution used for the flexural unloading model of ten Brink et al. [11]. (c) Crustal thickness variations and sedimentary basins used for modeling the gravity of the crustal thickening model. The predicted gravity has been tied to the observed gravity at km 630.

Moving the thermal boundary 50 km further inland only slightly improves the fit. The calculated gravity anomaly does not match the shape and amplitude of the observed gravity anomaly between the Wilkes Subglacial Basin and the Transantarctic Mountains. Similarly, the predicted gravity of a transitional boundary is difficult to match with our new gravity data.

The gravity model along the EAST93 traverse by ten Brink et al. [11] did not cover the transition into the Ross Embayment, which is a crucial constraint for the modeling (Fig. 7a). Because the modeled thermal boundary is located outside the area with gravity data and the length of the profile (300 km) is comparable to the depth of the sources (250 km), the gravity model by ten Brink et al. [11] is only weakly constrained. In summary, using a thermal low-density structure associated with the boundary between the Ross Embayment and the Transantarctic Mountains as suggested by ten Brink et al. [11] makes it difficult to match our new gravity data with the modeled gravity.

The low density material beneath the Transantarctic Mountains may reflect crustal thickening there, or it could be due to lateral variations in crustal or mantle density [30]. We have calculated the crustal thickening necessary to match the observed and modeled free-air gravity anomaly (Fig. 7). For simplicity, we assume that the long-wavelength variations of the gravity anomaly are predominantly caused by the topography of the crust–mantle boundary. For this reason we constrain the crustal thickness variations along the profile by fitting the long-wavelength components of the predicted gravity to the observed gravity. Our intention is to keep the gravity model as simple as possible. Over the Transantarctic Mountains, a thin low-density layer of Beacon sediments improves the short-wavelength fit (Fig. 7), which is in agreement with results from previous studies [11]. The density of the Beacon sediments has been estimated by laboratory measurements to be 2400 kg/m^3 [31]. The overall contribution of the Beacon sediments to the mod-

eled gravity is small (less than 6 mGal). For this reason, the uncertainty of the aerogravity data (3 mGal) prevents a reliable estimate of the subglacial extent of the Beacon sediments from gravity modeling alone, since the gravity contributions from a thin layer of Beacon sediments further inland will be smaller than the uncertainty in the data. A 4-km-thicker crust beneath the region with highest topography in the Transantarctic Mountains is necessary to match the modeled and observed gravity (Fig. 7).

The crustal thickening necessary to fit the gravity anomalies (4 km) is smaller than the root calculated from an Airy model (~8 km). The crustal root estimated from gravity modeling could not support the observed topography of the Transantarctic Mountains. For this reason additional forces for uplift are necessary. Certainly, erosional unloading of the Transantarctic Mountains, flexurally linked to the interior of the mountains, can be a major contribution to the uplift. Without reliable seismic constraints, gravity modeling alone cannot distinguish between the different models. The resolution of the most recent seismic tomography model [32] is around 400–700 km, depending on the wavelength of the seismic phases, and is not sufficient to resolve ten Brink et al.'s [11] hypothesized thermal boundary.

4.2. Wilkes Subglacial Basin

The Wilkes Subglacial Basin was originally referred to as a topographic depression and later interpreted as a sedimentary basin with up to 3–4 km of infill [8–10] or as a hinterland flexural basin, formed by regional isostatic response of a semi-infinite elastic plate to uplift of the Transantarctic Mountains [7,11,33]. Within our survey area, the proposed sedimentary basin lies between km 600 and 700 (Fig. 6). The observed free-air anomaly in this region does not support a low density infill. In contrast, the modeled gravity is smaller than the observed gravity requiring either a near-surface high density body or a Moho uplift necessary to match the modeled and observed gravity. Using a detection threshold of three times the standard deviation of the uncertainty in our aerogravity data (9 mGal) we could resolve a 1200-m-thick sediment layer with a density of 2400 kg/m^3. According to our data resolution the maximum possible sediment thickness within the Wilkes Subglacial Basin is less than 1 km.

The thickness of the sediment cover in the Wilkes Subglacial Basin can also be estimated from magnetic data. Magnetic data are often used to estimate the depth to the top of the causative magnetic source, which can be the depth of the magnetic basement, underlying a non-magnetic sediment layer. In order to estimate the magnetic basement depth along the transect we use Werner deconvolution. The depth to the top of a thin sheet like body or a magnetic contact and their respective magnetizations can be estimated from a profile of total-field measurements over the causative body [34,35]. The observed magnetic anomaly is analyzed in terms of the magnetic field of either a dike or a magnetic contact. Individual depth estimates tend to cluster vertically beneath the true location of the causative body.

Fig. 8 shows the depth estimates obtained from Werner deconvolution of a profile in the center of the survey area. The size of the individual circles is proportional to the magnetization of the Werner solution. Over the eastern half of our survey area (km 500–1050) several vertical 'streaks' of depth solutions form the typical cluster indicating a stable depth estimate (Fig. 8b). The top of the depth solutions coincides with the subglacial topography within a 1-km uncertainty estimate (km 500–1050 in Fig. 8b). The correspondence of the depth solutions with the subglacial topography indicates that the magnetic basement is coincident with the ice/bedrock contact within the confidence limit. A maximum of 1 km of sediments is possible in this region, unless a widespread magmatic event intruded the basin. If non-magnetic sediments exist in this region they must be intruded by widespread and dense post-depositional magnetic intrusions reaching the ice/bedrock interface. Such a pattern of magnetic intrusions could create a similar picture of depth solutions like a continuous shallow magnetic basement as seen in Fig. 8b. However, in the Ross Embayment, where several km thick sedimentary sequences are intruded by numerous Cenozoic volcanics, the sediment thickness could be estimated reliably from Werner

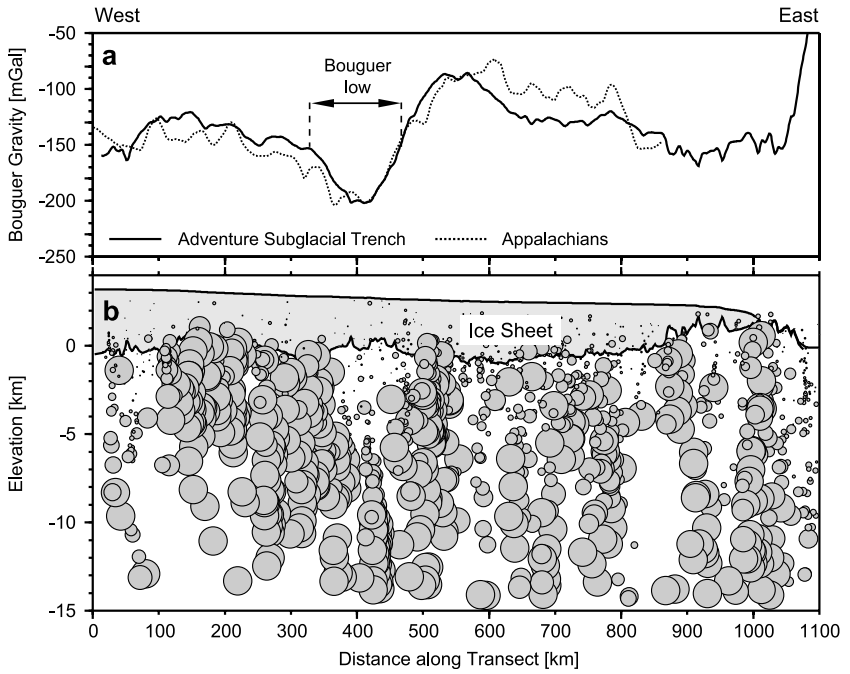

Fig. 8. (a) Comparison between the Bouguer gravity across the Adventure Subglacial Trench (solid) and the Appalachians (dashed), a thrust-and-fold belt, plotted at the same scale. The Appalachian gravity data have been uniformly shifted down in order to aid comparison. (b) Depth solutions from Werner deconvolution of magnetic data. The circles indicate individual depth solutions with the size being scaled to the magnetic susceptibility of the magnetic contact.

deconvolution [12]. The Werner deconvolution of the magnetic data supports the interpretation of little or no sediment infill within the Wilkes Subglacial Basin.

4.3. *Adventure Subglacial Trench and Resolution Subglacial Highlands*

To the west of 143°E, the trends of the magnetic, gravity and topography shift to northwest–southeast. We interpret the Resolution Subglacial Highlands and the Adventure Subglacial Trench as a tectonic unit based on the consistent trends and the coherent nature of the potential field and topography data. In order to constrain the crustal structure beneath the Resolution Subglacial Highlands and the Adventure Subglacial Trench we use gravity modeling. Our modeled gravity of both an Airy and flexural unloading model produces a 50-mGal misfit between kilometer 350 and 500 (Fig. 6). The sharp change in the observed gravity near kilometer 350 and 450 requires a shallow low-density body to match the observed and modeled gravity. The observed short-wavelength change in gravity cannot be modeled by a change in crustal thickness (Fig. 7).

Further support for sediment infill comes from depth estimates of the Werner solutions. Between km 350 and 500, the top of the depth solutions is around 5 km below sea level (Fig. 8). This region of deeper magnetic basement coincides with a low in Bouguer gravity (Fig. 8). The coinciding structure in Bouguer gravity and magnetic basement supports the concept of a low-density, non-magnetic material, making the presence of a 5-km-thick, 150-km-wide sediment infill likely. Interestingly, this sediment structure is just located eastward of the Adventure Subglacial Trench, and forms the eastern shoulder of the trench. The Adventure Subglacial Trench itself and the region west of it show a shallow magnetic basement which coincides with the ice/bedrock interface.

The high-amplitude magnetic anomalies between km 100 and 350 cause a dense clustering of depth solutions with high susceptibility in this region.

The large distance (>600 km) to the nearest rock outcrops allows only a tentative interpretation regarding the origin and nature of the Adventure Subglacial Trench. The regional Bouguer gravity anomaly plays an important role in understanding the geological nature of the Adventure Subglacial Trench. The Bouguer gravity anomaly is characterized by a adjacent high and low, with a peak-to-through amplitude of around 125 mGal (Fig. 8a, km 300–700). The components of this negative-positive couple have similar wavelength and amplitude, suggesting that they are related. This positive–negative dipole pattern is often observed over major thrust-and-fold belts like the Appalachians and the Alps (e.g. [36,37]). The long-wavelength negative gravity component is associated with the flexure of the basement while the positive gravity anomaly is the result of the crustal block overthrusted onto the underlying crust [36,38]. Fig. 8 illustrates the strong similarity between the gravity anomaly across the Adventure Subglacial Trench and the Appalachians. The crustal structure beneath the Adventure Subglacial Trench as inferred from gravity modeling and Werner deconvolution is consistent with a compressional scenario.

Several authors have suggested that the transition from the Transantarctic Mountains to the East Antarctic craton is near the western edge of the Wilkes Subglacial Basin and the Adventure Subglacial Trench (e.g. [10] and references herein). The transition to the East Antarctic craton has been mapped in northern Victoria Land. Within northern Victoria Land Flöttmann et al. [39,40] observed the Wilson Terrane overthrusted onto the East Antarctic craton. The orientation of these thrust faults is parallel to the orientation of the Adventure Subglacial Trench.

5. Discussion

Our analysis and interpretation of new aerogeophysical data is discussed in light of previous models for the origin of the Wilkes Subglacial Basin and the Adventure Subglacial Trench. Finally, we speculate on an alternative scenario for the formation of elevated topography in the Transantarctic Mountains.

The Wilkes Subglacial Basin has been previously interpreted as a hinterland flexural basin [7,11,33] whose origin is intimately linked with the uplift of the Transantarctic Mountains. The flexural basin predicted from modeling is approximately between km 220 and 790 (Fig. 6b). Stern and ten Brink proposed a flexural origin of the Wilkes Subglacial Basin based on the correspondence between the predicted topography and the observed topography ([7], Fig. 7 herein). However, we believe that the small amplitude of the predicted depression (320 m between the outer low near km 645 and the high near km 220) is too small to be isolated from pre-existing relief resulting from erosion or sedimentation. Fig. 6 shows that the Wilkes Subglacial Basin and the Adventure Subglacial Trench occupy most of the western part of the predicted flexural basin. The obvious mismatch between the predicted flexural basin and the observed topography underlines the importance of considering the influence of pre-existing structures in future models of the Wilkes Subglacial Basin. The axis and location of the Wilkes Subglacial Basin follow the geologic boundary between the Transantarctic Mountains and the Wilkes Subglacial Basin. We suggest a structural control of the basin rather than a simple flexural origin based on the basin trend and morphology. Furthermore, the complex form of the Wilkes Subglacial Basin indicates a simple coupled flexural origin for the Transantarctic Mountains and the hinterland basin is unlikely. The Wilkes Subglacial Basin narrows from more than 500 km at 75°S to less than 100 km near 83°S, while the Transantarctic Mountains are a relatively uniform feature (Fig. 1). If the Wilkes Subglacial Basin is a simple flexural response to the uplift of the Transantarctic Mountains, the basin wavelength should also be uniform.

The Adventure Subglacial Trench has previously been interpreted to be underlain by rifted crust and having a sediment infill between 3 and 10 km within the trench [8–10]. This simple interpretation is complicated by the fact that the Bou-

guer gravity low is shifted to the east, outside the topographic low of the trench (Fig. 2). The 10-km sediment infill proposed by Ferraccioli et al. [10] forms the eastern shoulder of the trench and not the trench. No sediments are within the trench in their analysis. The offset between the trench in subglacial topography and the low in Bouguer anomaly makes the proposed simple rift scenario unlikely. Furthermore, the proposed Cenozoic rifting along the craton margin by Ferraccioli et al. [10] is unlikely in the context of Antarctica being surrounded by spreading centers since the fragmentation of Gondwana, which has created a predominantly compressional stress field.

The possibility that a significant fraction of the high elevation of the Transantarctic Mountains may be supported by a crustal root raises the question of the origin of that root. We speculate [41] that West Antarctic structure, geologic history and heat flow may be consistent with the collapse of a high plateau of thick crust. In this scenario, the Transantarctic Mountains would have been on the edge of a plateau prior to the collapse. Extensional collapse of the hotter, therefore weaker, central part of the plateau would thin the crust there producing the Ross Sea. The cooler, stronger plateau edges, with slightly thicker than normal crust, would be left behind as the elevated Transantarctic Mountains.

6. Conclusions

Gravity, magnetic and subglacial topography maps have been compiled from 21 000 km of aerogeophysical measurements. The maps provide the most detailed picture of the structure behind the Transantarctic Mountains to date. Variations in gravity, topography and magnetic character outline the boundaries of several geologic and tectonic segments within the survey area. The coherent pattern in magnetic data and mesa topography suggests a subglacial extent of the Transantarctic Mountains 400–500 km inland of the last exposed rock outcrops. The western boundary of this tectonic unit coincides with the axis of the Wilkes Subglacial Basin. Based on gravity modeling and source depth estimates from magnetic data, we estimate that the maximum thickness of a potential sediment infill in the Wilkes Subglacial Basin is less than 1 km. To the west of the Transantarctic Mountains–Wilkes Subglacial Basin unit, the trends of the magnetic, gravity and topography shift to northwest–southeast. We interpret the Resolution Subglacial Highlands and the Adventure Subglacial Trench as a coherent tectonic unit defined by the northwest–southeast trends and the coherent nature of the potential field and topography data. A coinciding structure in gravity models and magnetic source depth estimates suggests a 5-km-thick and more than 100-km-wide sedimentary infill near the eastern shoulder of the Adventure Subglacial Trench. The crustal structure and the strong similarity of the observed gravity with the Appalachians suggest a compressional scenario for the origin of the Adventure Subglacial Trench and the Resolution Subglacial Highlands.

The modeled gravity using a local compensation fits the gravity data better than the previous model of a flexural unloading suggested by ten Brink et al. [11]. The modeled gravity using a thermal boundary is difficult to reconcile with our new gravity data. However, without reliable seismic control it is impossible to distinguish between our crustal thickening model and the thermal boundary suggested by ten Brink et al. [11].

The complexity and apparent structural control of the Wilkes Subglacial Basin, together with an alternative explanation for the observed gravity suggest, that a reassessment of the existing uplift models is necessary. In addition to the flexural uplift model, crustal thickening, underplating, and the collapse of a high plateau should be included in future studies of the formation of the Transantarctic Mountains.

Acknowledgements

We thank the US National Science Foundation's Support Office for Aerogeophysical Research for data acquisition, support, and reduction of the ice-penetrating radar data. Robert Arko (LDEO) is thanked for reducing the GPS, gravity, and magnetic data. Uri ten Brink and

Michel Diament are thanked for reviews. We thank the Italian Antarctic Programme (PNRE) for critical logistic support. Funding was provided by the US National Science Foundation (OPP #9615704). This is LDEO contribution 6569. *[VC]*

References

[1] E.J. Jankowski, D.J. Drewry, The structure of West Antarctica from geophysical studies, Nature 291 (1981) 17–21.
[2] I.W.D. Dalziel, D.H. Elliot, West Antarctica; problem child of Gondwanaland, Tectonics 1 (1982) 3–19.
[3] F. Tessensohn, G. Wörner, The Ross Sea rift system, Antarctica; structure, evolution and analogues, in: M.R.A. Thomson, J.A. Crame, J.W. Thomson (Eds.), Geological Evolution of Antarctica; Proceedings of the Fifth International Symposium on Antarctic Earth Sciences, International Symposium on Antarctic Earth Sciences 5, Cambridge University Press, Cambridge–New York, 1991, pp. 273–277.
[4] T.J. Wilson, Mesozoic and Cenozoic kinematic evolution of the Transantarctic Mountains, in: K. Kaminuma, Y. Yoshida, K. Shiraishi (Eds.), Recent Progress in Antarctic Earth Science, Terra Publications, Tokyo, 1992, pp. 304–314.
[5] T.J. Wilson, Cenozoic transtension along the Transantarctic Mountains, West Antarctic rift boundary, South Victoria Land, Antarctica, Tectonics 14 (1995) 531–545.
[6] P.G. Fitzgerald, M. Sandiford, P.J. Barrett, A.J.W. Gleadow, Asymmetric extension associated with uplift and subsidence in the Transantarctic Mountains and Ross Embayment, Earth Planet. Sci. Lett. 81 (1986) 67–78.
[7] T.A. Stern, U.S. ten Brink, Flexural Uplift of the Transantarctic Mountains, J. Geophys. Res. 94 (1989) 10315–10330.
[8] D.J. Drewry, Sedimentary basins of the East Antarctic Craton from geophysical evidence, Tectonophysics 36 (1976) 301–314.
[9] R.H.N. Steed, D.J. Drewry, Radio-echo sounding investigations of Wilkes Land, Antarctica, in: C. Craddock (Ed.), Antarctic Geoscience, International Union of Geological Sciences. Series B, vol. 4, Oslo, Norway, 1982, pp. 969–975.
[10] F. Ferraccioli, F. Coren, E. Bozzo, C. Zanolla, S. Gandolfi, I.E. Tabacco, M. Frezzotti, Rifted(?) crust at the East Antarctic Craton margin; gravity and magnetic interpretation along a traverse across the Wilkes Subglacial Basin region, Earth Planet. Sci. Lett. 192 (2001) 407–421.
[11] U.S. ten Brink, R.I. Hackney, S. Bannister, T.A. Stern, Y. Makovsky, Uplift of the Transantarctic Mountains and the bedrock beneath the East Antarctic ice sheet, J. Geophys. Res. B 102 (1997) 27603–27621.
[12] G.D. Karner, M. Studinger, R.E. Bell, Paradoxical gravity anomalies of the Ross Sea, Antarctica, Geophys. Res. Abstr. 5 (2003) 02058.
[13] G.L. Mader, Dynamic positioning using GPS carrier phase measurements, Manuscr. Geod. 11 (1986) 272–277.
[14] L.E. Cordell, A scattered equivalent-source methods for interpolation and gridding of potential-field data in three dimensions, Geophysics 57 (1992) 629–636.
[15] V.A. Childers, R.E. Bell, J.M. Brozena, Airborne gravimetry; an investigation of filtering, Geophysics 64 (1999) 61–69.
[16] R.E. Bell, V.A. Childers, R.A. Arko, D.D. Blankenship, J.M. Brozena, Airborne gravity and precise positioning for geologic applications, J. Geophys. Res. B 104 (1999) 15281–15292.
[17] R.B. Harlan, Eötvös corrections for airborne gravimetry, J. Geophys. Res. 73 (1968) 4675–4699.
[18] R.L. Parker, Rapid calculation of potential anomalies, Geophys. J. R. Astron. Soc. 31 (1973) 447–455.
[19] C.R. Bentley, Configuration and structure of the subglacial crust, in: R.J. Tingey (Ed.), The Geology of Antarctica, Oxford Monographs on Geology and Geophysics 17, Oxford University Press, Oxford, 1991, pp. 335–364.
[20] J.C. Behrendt, D.J. Drewry, E. Janowski, M.S. Grim, Results from an aeromagnetic and radio echo ice-sounding survey over the Dufek Intrusion, Antarctica, in: R.L. Oliver, P.R. James, J.B. Jago (Eds.), Antarctic Earth Science; Fourth International Symposium, Cambridge Univ., Cambridge, 1983, 508 pp.
[21] W. Bosum, D. Damaske, N.W. Roland, J. Behrendt, R. Saltus, The GANOVEX IV Victoria Land/Ross Sea Aeromagnetic Survey: Interpretation of Anomalies, Geologisches Jahrbuch E38 (1989).
[22] W.R. Roest, J. Verhoef, M. Pilkington, Magnetic interpretation using the 3-D analytic signal, Geophysics 57 (1992) 116–125.
[23] M.N. Nabighian, The analytic signal of two-dimensional magnetic bodies with polygonal cross-section; its properties and use for automated anomaly interpretation, Geophysics 37 (1972) 507–517.
[24] M. Pilkington, J.A. Percival, Crustal magnetization and long-wavelength aeromagnetic anomalies of the Minto Block, Quebec, J. Geophys. Res. B 104 (1999) 7513–7526.
[25] R.H.N. Steed, Structural interpretations of Wilkes Land, Antarctica, in: R.L. Oliver, P.R. James, J.B. Jago (Eds.), Antarctic Earth Science; Fourth International Symposium, Cambridge Univ., Cambridge, 1983, pp. 567–572.
[26] D.R. Pederson, G.E. Montgomergy, L.D. McGinnis, C.P. Ervin, H.K. Wong, Aeromagnetic survey of Ross Island, McMurdo Sound, and the Dry Valleys, in: L.D. McGinnis, (Ed.), Dry Valley Drilling Project, Antarctic Research Series 33, American Geophysical Union, Washington, DC, 1981, pp. 7–24.
[27] C. Bull, E. Irving, I. Willis, Further palaeomagnetic re-

sults from south Victoria Land, Antarctica, Geophys. J. 6 (1962) 320–336.
[28] S. Pondrelli, A. Amato, M. Chiappini, G.B. Cimini, D. Colombo, M. Di Bona, ACRUP1 Geotraverse; contribution of teleseismic data recorded on land, in: C.A. Ricci (Ed.), The Antarctic Region; Geological Evolution and Processes; Proceedings of the VII International Symposium on Antarctic Earth Sciences, International Symposium on Antarctic Earth Sciences 7, Terra Antartica Publication, Siena, 1997, pp. 631–635.
[29] D.L. Turcotte, G. Schubert, Geodynamics, Cambridge University Press, Cambridge, 2002, 456 pp.
[30] A.G. Smith, D.J. Drewry, Delayed phase change due to hot asthenosphere causes Transantarctic uplift?, Nature 309 (1984) 536–538.
[31] P.J. Barrett, P.C. Froggatt, Densities, porosities, and seismic velocities of some rocks from Victoria Land, Antarctica, N.Z. J. Geol. Geophys. 21 (1978) 175–187.
[32] M.H. Ritzwoller, N.M. Shapiro, A.L. Levshin, G.M. Leahy, Crustal and upper mantle structure beneath Antarctica and surrounding oceans, J. Geophys. Res. B 106 (2001) 30645–30670.
[33] U. ten Brink, T. Stern, Rift Flank Uplifts and Hinterland Basins – Comparison of the Transantarctic Mountains with the Great Escarpment of Southern Africa, J. Geophys. Res. 97 (1992) 569–585.
[34] S. Werner, Interpretation of magnetic anomalies at sheet-like bodies, Sveriges Geologiska Undersøkning Arsbook 43 (1953).
[35] C.C. Ku, J.A. Sharp, Werner deconvolution for automated magnetic interpretation and its refinement using Marquardt inverse modeling, Geophysics 48 (1983) 754–774.
[36] G.D. Karner, A.B. Watts, Gravity anomalies and flexure of the lithosphere at mountain ranges, J. Geophys. Res. 88 (1983) 449–477.
[37] H. Lyon-Caen, P. Molnar, Gravity anomalies, flexure of the Indian Plate, and the structure, support and evolution of the Himalaya and Ganga Basin, Tectonics 4 (1985) 513–538.
[38] G.S. Stockmal, C. Beaumont, Geodynamic models of convergent margin tectonics; the southern Canadian Cordillera and the Swiss Alps, in: C. Beaumont, A.J. Tankard (Eds.), Sedimentary basins and basin-forming mechanisms, Atlantic Geoscience Society Special Publication 5, Atlantic Geoscience Society, Halifax, NS, 1987, pp. 393–411.
[39] T. Flöttmann, G. Kleinschmidt, Opposite thrust systems in northern Victoria Land, Antarctica; imprints of Gondwana's Paleozoic accretion, Geology 19 (1991) 45–47.
[40] T. Flöttmann, G.M. Gibson, G. Kleinschmidt, Structural continuity of the Ross and Delamerian orogens of Antarctica and Australia along the margin of the paleo-Pacific opposite thrust systems in northern Victoria Land, Antarctica; imprints of Gondwana's Paleozoic accretion, Geology 21 (1993) 319–322.
[41] M. Studinger, W.R. Buck, R.E. Bell, Subice geology inland of the Transantarctic Mountains and uplift scenarios in light of new aerogeophysical data, EOS Transactions AGU Fall Meeting Supplement 83 (2002) Abstract T51A-1117.
[42] M.B. Lytte, D.G. Vaughan, BEDMAP-Consortium, BEDMAP – bed topography of the Antarctic, British Antarctic Survey, Cambridge, 2000.